Proceedings of ASME Turbo Expo 2015: Turbine Technical Conference and Exposition
GT2015
June 15 – 19, 2015, Montréal, Canada

GT2015-43949

Near-Hole Thermal Field Measurements for Round Compound Angle Film Cooling Holes Fed by Cross-flow

John W. McClintic, Ellen K. Wilkes, and David G. Bogard
The University of Texas at Austin
Austin, Texas, USA

Jason E. Dees
GE Global Research
Niskayuna, New York, USA

Gregory M. Laskowski and Robert Briggs
GE Aviation
Cincinnati, Ohio, USA

ABSTRACT

The effectiveness of film cooling from short cooling holes, scaled to engine conditions, has been shown to be dependent on the nature of the internal coolant feed. A common method of supplying coolant to film cooling holes in engine components is through an internal cross-flow, which causes skewed effectiveness profiles on the surface of film cooled parts. For round axial holes, this effect causes coolant jets to more effectively spread across the surface. Additionally, for compound angle round holes, the direction of the cross-flow relative to the direction of injection has a substantial effect on film cooling effectiveness. A cross-flow directed counter to the span-wise direction of coolant injection has previously been shown to cause greater lateral jet spreading than cross-flow directed in-line with the span-wise injection direction. To better understand the phenomena responsible for the improved coolant spreading, two-dimensional thermal field profiles were measured downstream of compound angle film cooling holes fed by an internal cross-flow. A smooth-walled rectangular channel was used to produce an internal cross-flow in both a counter and in-line flow direction. Thermal field cross-section data was collected at three stream-wise locations: 0.7, 3.4, and 8.8 diameters downstream of the holes. Blowing ratios of 0.75 and 1.00 were studied at a density ratio of 1.5. Experiments were performed in a low speed recirculating wind tunnel at high mainstream turbulence with a thick approach boundary layer relative to the film cooling holes. It was found that the improved lateral spreading observed in the coolant jets fed by a counter cross-flow occurred due to the formation of a bulge on the downstream side of the jet.

INTRODUCTION

Modern gas turbine engines typically operate at turbine inlet temperatures that exceed the allowable metal temperature for the hot gas path components. It is therefore necessary to actively cool the parts exposed to the hot combustion products. To do so, cooler air is redirected from the late compressor stages and routed through the hot gas path components to protect them from the extreme thermal conditions. For high heat load parts, film cooling, a process in which the cool air is injected through discrete holes in the hot gas path components at an angle such that it spreads out on the surface of the part, is often used to provide additional cooling and protection from the hot external flow.

The performance of film cooling is often quantified using a parameter called adiabatic effectiveness, which is the normalized adiabatic wall temperature of the film-cooled part. It is defined as follows:

$$\eta \equiv \frac{T_{aw} - T_\infty}{T_{c,exit} - T_\infty} \quad (1)$$

where T_{aw} is the adiabatic wall temperature, the temperature that is generally assumed to be the driving temperature for heat transfer into a film cooled part. Adiabatic effectiveness can also be understood as a measure of how well a coolant jet spreads out and protects the surface of the part. It has been found to vary considerably with different cooling hole configurations, shapes, and blowing rates.

To better understand why adiabatic effectiveness varies for different film cooling configurations and conditions, it is useful to measure the temperature field above the film cooled surface. It is helpful to recognize that the adiabatic effectiveness is just the footprint of the coolant jet, which exists above the wall. The temperature field above the wall shows how the coolant spreads out above the wall, which indicates how it interacts with the mainstream flow, and the direction in which it disperses. These temperatures can be normalized in the same manner as the adiabatic wall temperature:

$$\theta \equiv \frac{T - T_\infty}{T_{c,exit} - T_\infty} \quad (2)$$

The cooling hole geometry under consideration for this study is round compound angle holes. While axial holes are preferred in most applications, it is often necessary to use compound angle injection in highly curved regions on an airfoil to allow for an appropriately shallow injection angle [1]. There have been a number of studies, [2], [3], [4], and [5], that have

shown increased adiabatic effectiveness at higher injection rates when round compound angle holes are used instead of round axial holes. Compound angle holes perform more effectively at high blowing ratios because the compound angle jet presents a larger cross-section to the mainstream flow than axial jets, allowing the mainstream flow to more effectively force the jet down towards the wall. Therefore, jets from axial holes will separate from the wall at lower coolant flow rates than compound angle jets. Ligrani *et al.* [4] measured thermal fields downstream of compound angle film cooling holes, and showed the compound angle jets remaining better attached to the wall relative to jets from round axial holes. Unlike the axial jets, which had symmetric jet profiles, the compound angle jets were asymmetric and tilted toward the downstream side of the jet at x/d = 9.9. The difference between the effectiveness of compound angle holes and axial holes demonstrates the importance of considering how jets develop above the wall.

The development of the coolant jet above the wall has been examined in several experimental studies. Andreopoulis and Rodi [6] performed detailed flow field measurements of a jet issuing from a hole twelve diameters long, injected normally into the mainstream. The flow field measurements showed a kidney-shaped counter-rotating vortex pair developing as a result of the mainstream deflecting around the jet at the point of injection, the strength of which was dependent on the velocity ratio between the coolant jet and the mainstream. This vortex pair allowed for a considerable rate of ingestion of mainstream air under the jet. However, the length of the hole used in this study was much longer than what would be seen in typical engine components. Pietrzyk *et al.* [7] made detailed velocity measurements in the near-hole region of a hole that was only 3.5 hole diameters in length, which is a more realistic configuration. Their flow field measurements also showed a high degree of mainstream ingestion underneath the coolant jet. They also concluded that a separation region developed near the entrance of the shorter hole that led to high turbulence levels in the hole that had not been observed in earlier studies with longer coolant holes.

A number of computational studies have also been performed to predict how the hole exit condition affects vortex development downstream. Leylek and Zerkle [8] found that, for short film cooling holes, differences in the coolant feed condition affect how coolant exits the cooling hole and therefore affect how the coolant spreads out along the surface of the film cooled part. Walters and Leylek [9] traced the origins of the counter rotating vortex pair observed by Andreopoulis and Rodi [6] and found that it was primarily caused by stream-wise oriented vorticity within the film holes. McGovern and Leylek [10] performed a similar computational study on compound angle round holes and showed that the symmetrical vortex pair that had been observed for axial round holes became increasingly asymmetrical with increasing compound angle. The strength of the upstream vortex was reduced under compound angle injection due to interaction with the mainstream, making the downstream vortex the stronger of the two.

The aforementioned studies all examined the performance of cooling holes fed by a quiescent plenum, which is a common method of supplying coolant for film cooling experiments and simulations. However, coolant in engine components is rarely supplied in this fashion. Internal coolant flow is commonly directed normal to the direction of the mainstream, which will be termed "internal cross-flow" hereafter. Thole *et al.* [11] measured the velocity field at the entrance and exit of holes fed by a co-flow (or internal flow parallel to the direction of the mainstream) at varying velocities. It was found that the co-flow caused a skewing of the velocity profile within the hole that varied with the strength of the co-flow. The skewed velocity profiles were the result of a separation bubble that formed at the inlet of the cooling hole, as predicted by Pietrzyk *et al.* [7]. A number of studies, including Gritsch *et al.* [12], [13], and Saumweber and Schulz [14] found that jets from round axial holes fed by an internal cross-flow exhibited greater lateral spreading and therefore higher adiabatic effectiveness levels than jets from round axial holes fed by a quiescent plenum. The performance of the cross-flow fed holes was most notably improved at higher blowing rates, similar to the effect of compound angle injection compared to axial injection. Dees *et al.* [14] also showed that axial round holes on a scaled up turbine vane model fed by a cross-flow had a skewed effectiveness profile. Interestingly, Gritsch *et al.* [13] found that the jets were skewed such that there was higher effectiveness on the windward side of the hole relative to the cross-flow direction, while Dees *el at* [15] observed the opposite trend. The difference between the two studies could have been caused by different cross-flow velocities relative to the mainstream flow. Gritsch *et al.* [13] tested at high speeds and had coolant to mainstream Mach number ratios of Ma_c/Ma_∞ = 1.0 and 2.0 while Dees *et al.* [15] tested at low speeds with a coolant to mainstream velocity ratio of U_c/U_∞ = 0.4. In an accompanying study, Dees *et al.* [16] performed thermal field measurements above the film cooling holes tested previously and showed a skewing of the jet shape that led to better attachment on the leeward side of the jet.

A number of computational studies have been performed to better understand why cross-flow improves the performance of axial round holes. Saumweber and Schulz [14] found that cross-flow caused an asymmetric vortex pattern within the coolant hole that led to an asymmetric rotating vortex pair above the wall, which spread out the coolant more effectively in the span-wise direction. The coolant formed a spiral shaped pattern with the leeward side of the coolant jet separated from the wall. Another study by Peng and Jiang [17] also computationally predicted an asymmetrical vortex in the cooling hole that led to a more spread out and asymmetric jet when it was fed by an internal cross-flow. The asymmetric jet in that study was nearly divided into two separate jets with the leeward jet showing greater separation.

The first study of the effects of cross-flow on compound angle round holes was performed by McClintic *et al.* [18]. Adiabatic effectiveness measurements were performed for compound angle round holes fed by cross-flow in both

directions: counter to and in-line with the span-wise direction of coolant injection. It was found that counter cross-flow resulted in considerably higher peak effectiveness levels than in-line flow due to increased lateral spreading of coolant on the downstream side of the jets (corresponding to the leeward side of the hole relative to coolant injection). Klavetter [19] added a comparison to a quiescent plenum configuration and showed that while the plenum case performed similarly to the in-line configuration at low blowing rates, the plenum case had much lower effectiveness at higher blowing ratios, which is similar to the result seen by Gritsch *et al.* [13].

The purpose of this study is to provide better understanding of how cross-flow affects round compound angle holes by measuring two-dimensional thermal fields in the region just downstream of the cooling hole. Experimentally measured thermal fields for cross-flow fed jets are very rare in the literature and no such measurements exist for compound angle jets. There is also considerable value in experimental measurements of thermal fields given that computational predictions of thermal fields can be subject to large errors [20]. The configuration used in this study is the same as in McClintic *et al.* [18]: eight holes with an injection angle of 30° and a compound angle of 45° with a hole length of L/d = 6.0 and a hole spacing of p/d = 6.25. Coolant was provided through the same cross-flow channel at a channel inlet Reynolds number of Re_{ch} = 35,000 and a cross-flow to mainstream velocity ratio of 0.52. Experiments were conducted at density ratio of DR = 1.5 at low speed, high mainstream turbulence, and at blowing ratios of M = 0.75 and 1.00, which had the highest measured adiabatic effectiveness levels of the blowing ratios tested.

NOMENCLATURE

d	film cooling hole diameter
d_H	hydraulic diameter
DR	density ratio ρ_c/ρ_∞
H	boundary layer shape factor
I	momentum flux ratio $\rho_c U_c^2/\rho_\infty U_\infty^2$
k	thermal conductivity
L	film cooling hole length
L_e	development length
M	blowing ratio $\rho_c U_c/\rho_\infty U_\infty$
Ma	Mach number
p	film cooling hole pitch
Re	Reynolds number
t	wall thickness
T	total temperature
Tu	turbulence intensity $\sqrt{\overline{u'^2}}/\overline{U}$
U	velocity
x	stream-wise coordinate measured from downstream edge of cooling hole
y	wall-normal coordinate measured from the wall
z	span-wise coordinate measured from intersection of cooling hole edge with x = 0

GREEK

α	cooling hole injection angle
β	cooling hole compound angle
δ	boundary layer thickness, uncertainty
δ^*	boundary layer displacement thickness
η	adiabatic effectiveness
Λ_f	turbulence integral length scale
θ	normalized temperature, boundary layer momentum thickness
ρ	density

SUBSCRIPTS, ACCENTS

aw	adiabatic wall
b	bias uncertainty
c	coolant
ch	channel
p	precision uncertainty
∞	mainstream

EXPERIMENTAL FACILITIES AND PROCEDURES

DESCRIPTION OF FACILITIES

Data for this study were collected at The University of Texas at Austin in a closed-loop, low-speed wind tunnel powered by a 3.7 kW (5 hp) variable-speed motor. The test section, used to collect thermal field measurements for the investigated film cooling configuration, measured 138 mm high and 609 mm wide. The motor supplied a mainstream velocity of U_∞ = 13.8 m/s to the test section, corresponding to a Reynold's number of Re_d = 4,400 using the coolant hole diameter as the characteristic length corresponding to the Reynolds number for typical engine conditions (T_∞ = 1900 K and p_∞ = 28 atm) when the local mainstream Mach number is Ma_∞ = 0.14. A passive turbulence generator was installed sufficiently upstream of the test section to produce isotropic turbulence that was uniform across the span of the tunnel. The approach mainstream turbulence level was measured to be Tu = 4.5% with an integral length scale of Λ_f = 22.9 mm (4.6 times larger than the coolant hole diameter). The turbulence generator was made up of a series of vertical cylindrical rods spaced along the width of the tunnel designed to provide the desired mainstream turbulence level. Both the mainstream turbulence level and the ratio of the integral length scale to coolant hole diameter are typical of engine conditions across a first stage turbine blade.

The test section, shown in Figure 1, was designed to simulate film cooling from coolant holes on the low curvature region of the suction side of a turbine airfoil. To ensure the appropriate approach boundary layer upstream of the holes, a suction plenum was installed beneath the tunnel to remove the upstream boundary layer. A new boundary layer began to form from the stagnation point of the elliptical leading edge of the flat plate. To quicken the transition to a turbulent boundary layer, a 3.175 mm cylindrical rod, secured horizontally across

the width of the tunnel 38 mm downstream of the flat plate leading edge, was used to trip the flow. The trip produced a turbulent approach boundary layer with a specified thickness of δ/d = 2.8, a displacement thickness of δ^*/d = 0.36, a momentum thickness of θ/d = 0.27, and a shape factor of H = 1.33. To verify the conditions of the boundary layer, measurements of the velocity profile at the upstream edge of the coolant holes (152 mm downstream of the trip location) without film cooling were taken using a hot wire probe. The velocity profile, shown in Figure 2, was consistent with the 1/7 power law, indicating that the approach flow boundary layer was fully turbulent.

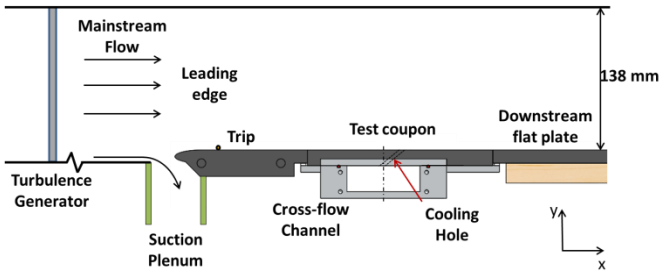

Figure 1: Schematic of wind tunnel test section

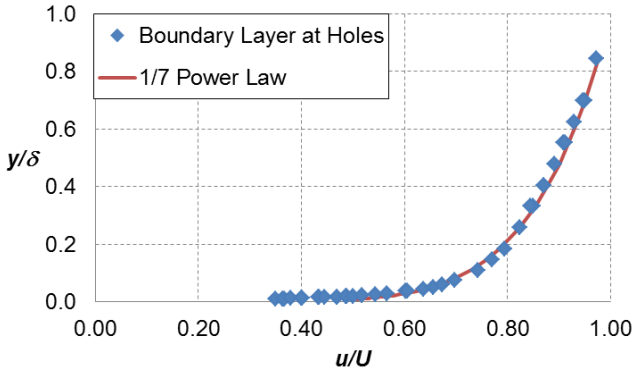

Figure 2: Profile of the approach boundary layer without film cooling

For film cooling experiments, coolant was delivered to the holes through a coolant loop connected to the wind tunnel, as shown in Figure 3. Coolant, in the form of liquid nitrogen, was supplied by a dewar to the coolant heat exchanger, where it was warmed to a gaseous state by mainstream tunnel gas provided by a 5.6 kW (7.5 hp) constant speed blower. The nitrogen gas was routed to a rectangular cross-flow channel secured beneath the flat plate to supply the nitrogen to the coolant holes. The nitrogen gas could flow in either direction through the channel by opening and closing certain valves in the piping system. The flow rate of nitrogen entering the channel was measured by an orifice flow meter calibrated according to an ASME standard, and could be controlled by the dewar. The flow rate of coolant through the holes was measured as the difference of mass entering and exiting the channel. The mass exiting the channel was measured by a Venturi flow meter, calibrated against the orifice flow meter to avoid bias errors in coolant flow rate calculations. By adjusting the mass flow rate of nitrogen entering the system and the flow rate of mainstream tunnel gas to the heat exchanger, the temperature and the flow rate of coolant through the channel could be altered independently. After exiting the channel, the nitrogen was exhausted into the main flow loop. Both the coolant flow loop and the channel had to be substantially insulated to prevent undesirable heat losses from the system. The mainstream temperature was set to T_∞ = 303 K and was held steady to ± 1 K throughout the experiment by use of the mainstream heat exchanger, which used hot water to keep the mainstream temperature from dropping due to continual coolant injection.

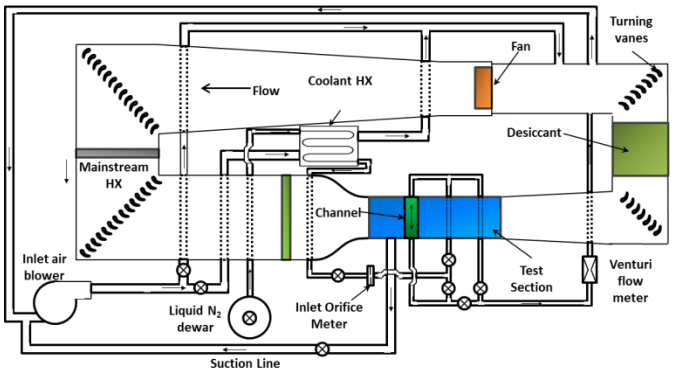

Figure 3: Schematic of wind tunnel and coolant flow loop

The coolant supply channel, installed beneath the coolant holes in the test section, shown in Figure 4, was 1680 mm long and constructed from aluminum, with a cross-section 70 mm wide by 25 mm high. For all experiments, the coolant flow rate through the channel was kept at an inlet Reynolds number of Re_{ch} = 35,000, calculated using the hydraulic diameter of the channel, d_H = 36.8 mm. This Reynolds number corresponded to an inlet internal cross-flow velocity of 7.2 m/s, which was 52% of the mainstream tunnel velocity. Due to coolant loss through the holes, the Reynolds number and internal flow velocity were reduced by 3-6%, depending on flow conditions, between the channel inlet and the hole at which measurements were performed. It was desired that the flow in the channel be fully developed turbulent flow upstream of the cooling hole inlets. To ensure these conditions, screens were fixed at the inlet of the channel to remove any upstream flow structures, and the channel was designed to have sufficient development length, L_e = 10.35d_H, such that the flow was fully developed by the time it reached the hole locations. To verify that the channel met the specified conditions, a velocity profile, shown in Figure 5, was measured 102 mm upstream of the channel test section location across the height of the channel. The velocity profile shown was independent of the direction of the flow through the channel. The profile was symmetric and compared well to both the 1/7 power law and long development length profiles. The long development length profile was measured when the channel flow was allowed to develop over the entire length of

the channel with the film holes blocked. Because the long development length and approach velocity profiles agreed within uncertainty, the channel approach length was sufficiently long enough to allow the flow to become fully developed.

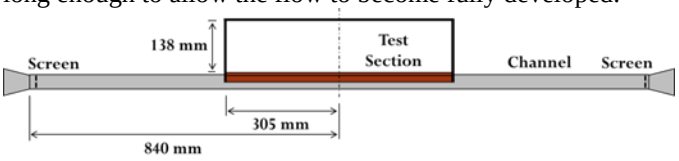

Figure 4: Schematic of coolant supply channel

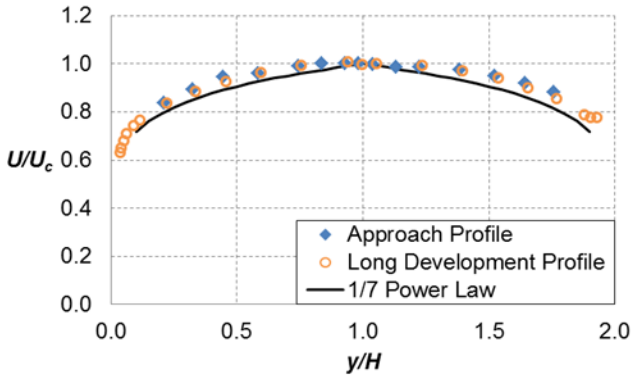

Figure 5: Velocity profile along the coolant channel centerline

As shown in Figure 6, there were two internal cross-flow directions tested in this study. Counter cross-flow is directed counter to the span-wise direction of coolant injection and in-line cross-flow is directed in-line with the span-wise direction of coolant injection. The terms "counter" and "in-line" will be used from now on to describe these two cross-flow directions.

A test coupon, with a thickness of t = 15 mm, was fabricated of low conductivity, closed cell polyurethane foam (k ≈ 0.048 W/m·K) to model the desired film cooling geometry. The test coupon fit above the coolant supply channel and housed eight cylindrical cooling holes through which coolant flowed from the channel into the tunnel. The holes had a diameter of d = 5 mm and a pitch p = 31.25 mm such that the hole spacing was p/d = 6.25. The holes were machined with a stream-wise injection angle of α = 30º and a compound angle of β = 45º. These parameters resulted in a coolant hole length to diameter ratio of L/d = 6. The coordinate system, pictured in Figure 6, was defined such that x = 0 at the downstream edge of the cooling hole outlet, y = 0 at the surface of the test coupon, and z = 0 at the intersection of x = 0 and the farthest downstream point of the cooling hole outlet. The coupon was installed into the test section so that it was level with the upstream and downstream edges of the test section and that any roughness caused by the junction between the surfaces was less than 0.1 mm. Care was taken to ensure that the test section floor was smooth and well-sealed.

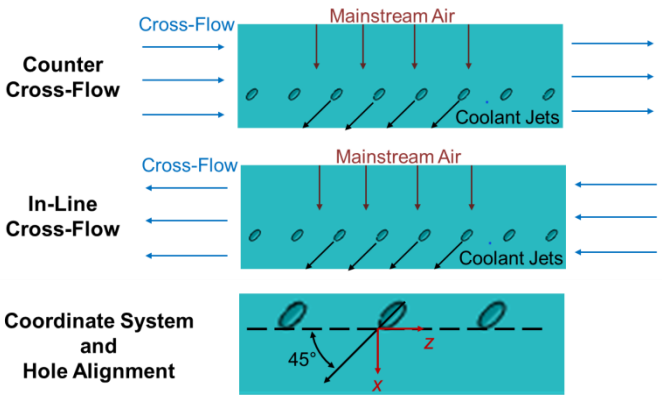

Figure 6: Cross-Flow Direction Terminology and Coordinate System

MEASUREMENT TECHNIQUES

Thermal field measurements of the coolant jets were made using a microthermocouple probe. The probe was constructed using a 0.05mm diameter, type E thermocouple wire secured to a repurposed hot film probe holder with a prong diameter of 0.3 mm. The probe holder was thoroughly insulated to prevent electrical conductivity between the wire and the probe base. The thermocouple junction was suspended between the two prongs of the probe holder to minimize conduction errors along the wire due to the thermal gradients in the coolant jets. The probe was calibrated against a range of known temperatures (258 K to 308 K) in a glycol-water bath. The calibration range was limited by the composition of the bath on the lower end and was enough to encompass all the data measured for θ < 0.44. While colder temperatures were measured with the probe, the calibration is expected to extrapolate well down to 248 K (θ = 0.54) based on similar previous calibrations. Given that the NIST calibration for E-type thermocouples is accurate down to 73 K, and that the measured calibration curve for this probe has low scatter and is linear, it is not expected that large errors are introduced by extrapolating down to the minimum temperatures measured: T = 217 K (θ = 0.85). Furthermore, the vast majority of the data collected in this study were at temperatures within the range of the probe calibration. The probe calibration was offset by about 2.0 K from the NIST E-type thermocouple calibration, as shown in Figure 7, but was repeatable to within ±0.05 K. The scatter in the probe calibration was ± 0.2 K. This scatter was primarily caused by fluctuations in the bath temperature at lower temperatures as it attempted to maintain the set temperature.

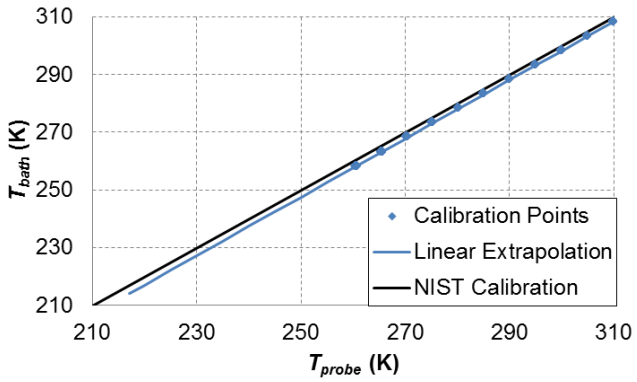

Figure 7: Microthermocouple probe calibration

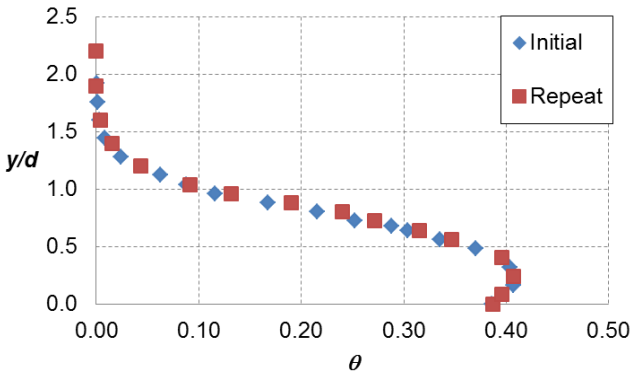

Figure 8: Thermal profile showing test-to-test repeatability for M = 0.75 at x/d = 3.35 and z/d = 0.21

An assembly of three Zaber model T-LSR traverses mounted above the test section was used to move the probe in a three dimensional space to collect thermal field measurements at three stream-wise positions downstream of the holes. Zaber states the accuracy of the traverses to be ± 15 µm. Thermal profiles were measured at x/d = 0.69, 3.35, and 8.77. At each x/d position, profiles at 15 different span-wise positions, from z/d = -2.4 to 3.86, were measured to capture the entire width of a pitch. The z-location of the probe was repeatable within z = ± 0.25 mm from test-to-test using a locating mark on the test surface. Each profile began with the probe in contact with the wall, at y/d = 0. The location of the wall was repeatable to within y = ± 0.05 mm. From this position, the probe was traversed upward from the wall in increments such that $|\Delta T| < 5$ K when the probe was moved upward. At each location, at least three measurements were made ensuring that the measured blowing ratio was within ± 0.05 of the target blowing ratio. All measurements made with a blowing ratio outside the acceptable range were removed during post-processing.

The temperatures of the mainstream gas and coolant were measured by E-type thermocouples. The mainstream thermocouples were calibrated with an accuracy of ± 0.04 K against the same glycol-water bath used to calibrate the microthermocouple probe. The mainstream thermocouples and microthermocouple probe agreed within ± 0.1 K when the probe was brought into the mainstream. The coolant thermocouples were not calibrated using the bath and instead, the NIST calibration was used. The coolant temperature, T_c, was calculated as the average of the channel inlet and outlet temperatures. This value of T_c has agreed with the temperature of the coolant exiting the holes within ± 1 K in past experiments. T_c was kept at approximately 202 K during experiments with the mainstream temperature at about 303 K, returning an appropriate density ratio. To prevent frost build-up around the coolant holes and in the channel, the wind tunnel was de-humidified prior to data collection by placing hot desiccant packs in the tunnel. A relative humidity of less than 3% was maintained throughout the course of the experiments.

The important flow parameters for this study: density ratio, blowing ratio, momentum flux ratio, and channel Reynolds number, were calculated from equations 3, 4, 5, and 6 respectively. Thermal fields were measured at two blowing ratios, M = 0.75 and 1.00, at both cross-flow directions, at a density ratio DR = 1.5. These parameters correspond to momentum flux ratios I = 0.38 and 0.67. As mentioned previously, the channel inlet Reynolds number was set to Re_{ch} = 35,000. During each experiment, the specified parameters were held steady. The density ratio was not allowed to vary more than ± 0.01, the nominal blowing ratio no more than ± 0.05, and the channel inlet Reynold's number no more than ± 1000. The experiments showed good in-test and test-to-test repeatability. Profiles at M = 0.75 from two different thermal field experiments are shown in Figure 8. The initial and repeat experiment show the same trend and the normalized temperature measurements agree within ± 0.01.

$$DR \equiv \frac{\rho_c}{\rho_\infty} \tag{3}$$

$$M \equiv \frac{\rho_c U_c}{\rho_\infty U_\infty} \tag{4}$$

$$I \equiv \frac{\rho_c U_c^2}{\rho_\infty U_\infty^2} \tag{5}$$

$$Re_{ch} \equiv \frac{\rho_c d_H U_{ch}}{\mu_c} \tag{6}$$

The thermal field measurements compared well to the normalized measured surface temperatures McClintic *et al.* [18], as shown in Figure 9. The normalized surface temperature contours are not corrected for conduction in order to reflect the actual surface temperatures that the probe was in contact with. Thermal fields measured at both blowing ratios have reasonable agreement with the surface measurements, further suggesting good repeatability for this facility. The thermal field profiles are slightly offset from the normalized surface temperature,

particularly farther away from the center of the jet in the span-wise direction. This could result from the inability of the microthermocouple to fully resolve the thermal boundary layer. Where IR thermography of the surface is negligibly influenced by gas flowing above the wall, the thermocouple probe is thick enough to be influenced by thermal gradients inside the boundary layer.

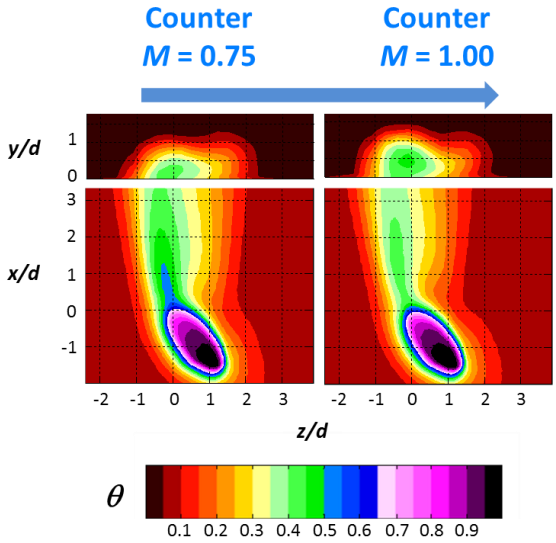

Figure 9: Thermal field profiles compared to normalized measured surface temperature [18]

The uncertainty in θ was dominated by unsteadiness in blowing ratio, which fluctuated from the mean by up to ± 0.06 during the experiments. This unsteadiness in blowing ratio caused the jets to move around slightly during the course of the experiments. Additionally, the coolant jets were subjected to high mainstream turbulence with large integral length scales, which has been shown in previous studies to cause jet oscillation [21]. This phenomenon has also been observed while viewing the test surface in this study with an IR camera. Due to unsteadiness in the coolant jets, the precision uncertainty of θ in regions of large temperature gradients, namely the shear layers on top of the jet was as high as $\delta\theta_p \leq \pm$ 0.05 at x/d = 0.69, which featured the largest temperature gradients. For the other stream-wise locations, the precision uncertainty of θ was no greater than $\delta\theta_p \leq \pm$ 0.013. In the jet core, the precision uncertainty was $\delta\theta_p \leq \pm$ 0.008 due to the reduced temperature gradients and turbulence levels. Outside the jets, the precision uncertainty was negligible and the probe was able to measure θ = 0 to within $\delta\theta_b = \pm$ 0.001, which is representative of the bias uncertainty in the probe. The uncertainty given above is the uncertainty for the measured data points. Interpolation errors were added to the data during the creation of the contour plots shown in Figure 12 due to the spacing of the profiles in the span-wise direction. The largest spacing between points in the region containing the jets was 1.5 mm or 0.3 hole diameters. The magnitude of the interpolation errors is dependent on the temperature gradients within the jets. Therefore, all non-contour plots of thermal field data measured for this study do not contain interpolated data.

The uncertainty in the measured blowing ratio was estimated using the sequential perturbation analysis of Moffat [22]. The bias uncertainty in blowing ratio was $\delta M_b = \pm$ 0.07 and was primarily caused by the fossilized bias in the Venturi meter calibration and the uncertainty in the cooling hole diameter and the flow meter throat diameters. The precision uncertainty was $\delta M_p = \pm$ 0.009 and was primarily the result of precision uncertainties in the Venturi pressure drop measurement and the temperatures in the flow meters. The uncertainty in the density ratio was $\delta DR = \pm$ 0.008, which was much lower than the variance imposed by tunnel operation.

RESULTS AND DISCUSSION

Thermal field measurements were made downstream of a row of round compound angle film cooling holes fed by an internal cross-flow directed both in-line with and counter to the span-wise direction of coolant injection. The temperature field measurements were collected in the y-z plane at three different stream-wise positions (x/d = 0.69, 3.35, and 8.77) in order to capture three different coolant jet cross-sections. The experiments were performed at a density ratio of DR = 1.5 and blowing ratios of M = 0.75 and 1.00 (I = 0.38 and 0.67).

Adiabatic effectiveness measurements for this configuration [18] showed that at M = 0.75 and 1.00, the counter cross-flow jets had higher laterally averaged adiabatic effectiveness due to improved coverage on the downstream side of the coolant jets. This result is evident in Figure 10, which shows contour plots of individual jets for the conditions tested in this study. The effectiveness distributions for the counter cross-flow cases are clearly broader than that for the in-line cross-flow cases. Lateral profiles of adiabatic effectiveness are shown in Figure 11 for M = 0.75 at the three stream-wise positions measured in this study for both in-line and counter flow. At the downstream positions (x/d = 3.35 and 8.77), the in-line and counter effectiveness profiles were nearly identical on the upstream side of the jet (negative z/d) but on the downstream side of the jet, the counter flow case had considerably higher adiabatic effectiveness. To obtain an understanding of why there was better laterally spreading of the coolant for the counter cross-flow cases, the thermal fields above the surface were measured to determine the distribution of coolant above the surface.

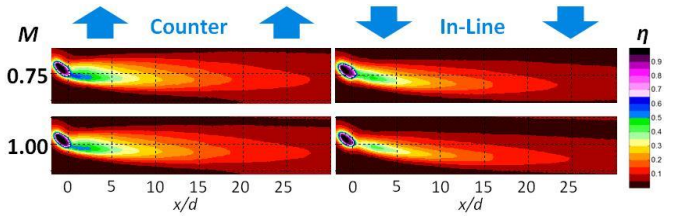

Figure 10: Contours of adiabatic effectiveness at the blowing ratios tested in this study [18]

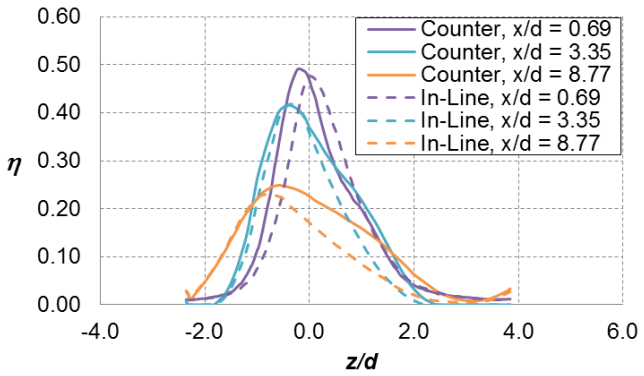

Figure 11: Lateral profiles of η at M = 0.75 at the stream-wise locations tested in this study [18]

Measurements of thermal fields showed that the counter cross-flow produced jets with increased lateral spreading on the downstream side of the jet. Figure 12 shows contour plots of the jets for all measured profiles in this study. The arrows at the top of the figure indicate the direction of internal cross-flow relative to the plots. The cross-section profiles clearly show that the improved lateral spreading for the counter cross-flow case was the result of a bulge on the right side of the jet. Note that the compound angle jets flow right to left, so mainstream impacts the left side of the jets, and the right side of the jets is the downstream side of the jets. The extension of the coolant to the right was such that it nearly formed a second jet core, which was initially separated from the wall, but appeared to attach to the wall and combine with the primary jet core farther downstream.

The in-line flow, however, has a considerably different jet shape than the counter flow jet at both blowing ratios. While it did show evidence of some lateral spreading at x/d = 0.69, the jet became more circular in shape further downstream. The shape of the in-line jet more closely resembled the shape of the jet thermal field measured by Ligrani *et al.* [4] for round compound angle holes fed by a quiescent plenum. Interestingly, the skewing of the in-line jet shape changed between x/d = 3.35 and 8.77, likely due to asymmetrical vortical motion within the jet.

The difference between the jets for the two cross-flow directions must have originated at the inlet of the coolant holes. As McClintic *et al.* [18] postulated, the counter flow case is likely to have experienced increased separation as it entered the coolant holes due to the sharper turn the coolant had to perform to enter the holes, while the in-line flow would have entered the hole more smoothly due to the more favorable turning angle. The manner of the coolant's entry into the holes would have determined how the flow developed within the holes and exited into the mainstream. The exit velocity and turbulence profile of the jet would have then influenced the development of the vortical structures within and around the coolant holes, which caused the observed temperature profiles. The difference in the vortical structures in the in-line and counter jets as they exited the hole also likely affected how the jets interacted with the mainstream. If the counter flow case featured a larger separation region within the coolant hole, the hole-exit velocity profile would likely have been more skewed, likely influencing the development of the observed downstream bulge. Because the in-line coolant likely entered the hole more smoothly, the jet would have exited with a more parabolic profile that allowed it to retain the circular cross-sectional shape expected for a jet

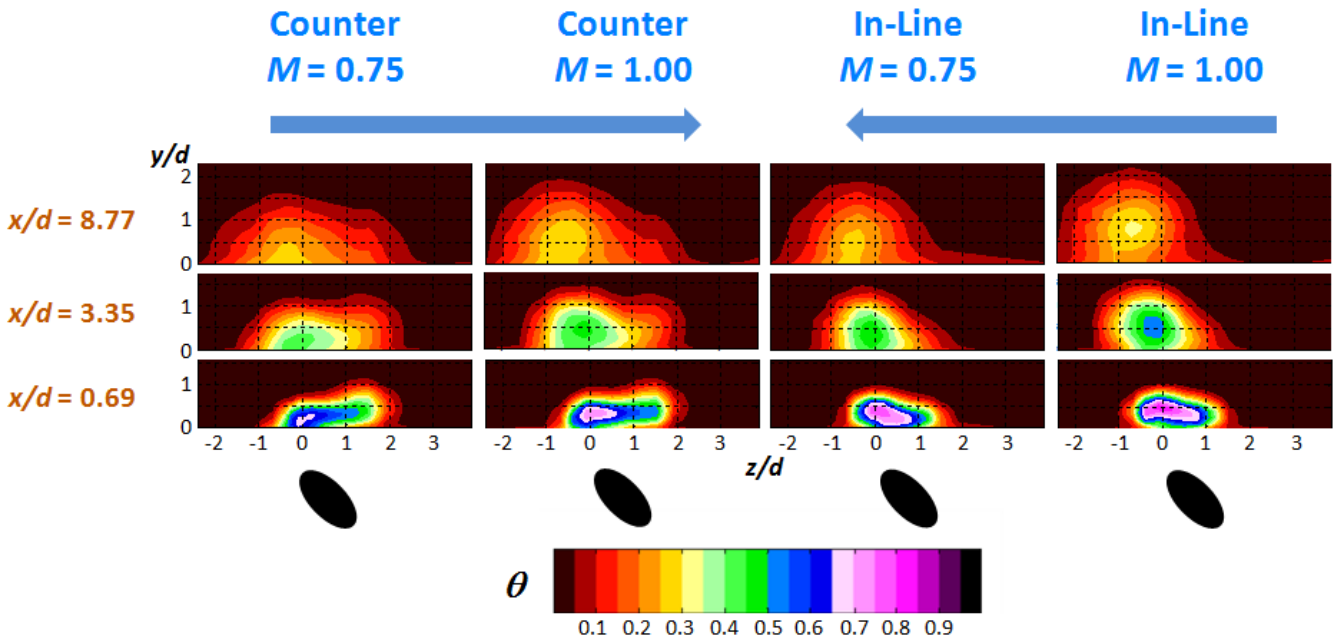

Figure 12: Cross-sections for all measured profiles

emerging from a cylindrical hole. While the downstream bulge in the counter flow case lost its shape and appeared to disperse further downstream, it resulted in a jet with greater lateral spreading than its in-line counterpart, and caused improved effectiveness for the counter cross-flow jet relative to the in-line case further downstream.

It can also be observed that the core temperature of the in-line jet was colder than the core temperature for the counter jet, which shows that the in-line jet remained better intact than the counter jet over the range of stream-wise locations tested. This result is demonstrated in Figure 13 which plots the normalized centerline temperatures of the jets for both cross-flow directions and blowing ratios at x/d = 3.35. At both blowing ratios the in-line jets had higher maximum θ (colder minimum temperatures) than the counter flow jets and the minimum temperatures for the in-line jets were further from the wall than those for the counter flow jets. This result indicates that the in-line jets stayed together more effectively than the counter jets and as a result had greater momentum, which caused them to more readily separate from the wall. These two phenomena had opposite effects on centerline adiabatic effectiveness. The open symbols in Figure 13 represent the normalized measured surface temperatures from [17]. The difference between the thermal field measurements and the surface temperature measurements at y = 0 was a result of the inability of the probe to fully resolve the thermal boundary layer in the steep temperature gradients near the wall. The centerline adiabatic effectiveness for the two cross-flow cases were roughly the same for M = 0.75 and 1.00 even though the core jet temperature were distinctly colder for the in-line cases. This was because the counter jets were better attached. Because the counter flow jet has better centerline attachment and more lateral spreading than the in-line flow jet, the laterally averaged adiabatic effectiveness was considerably higher than the laterally averaged adiabatic effectiveness of the in-line case as shown in Table 1.

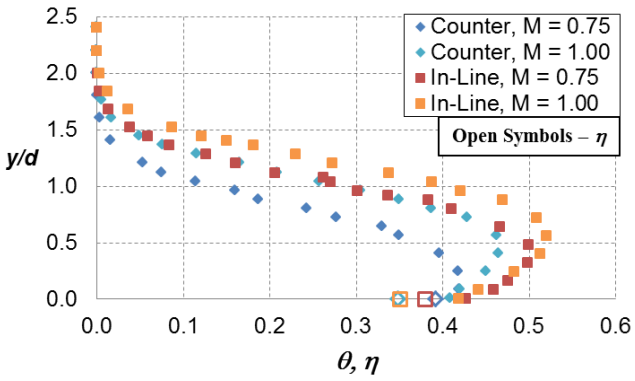

Figure 13: Centerline thermal profiles of the jets from all configurations at x/d = 3.35

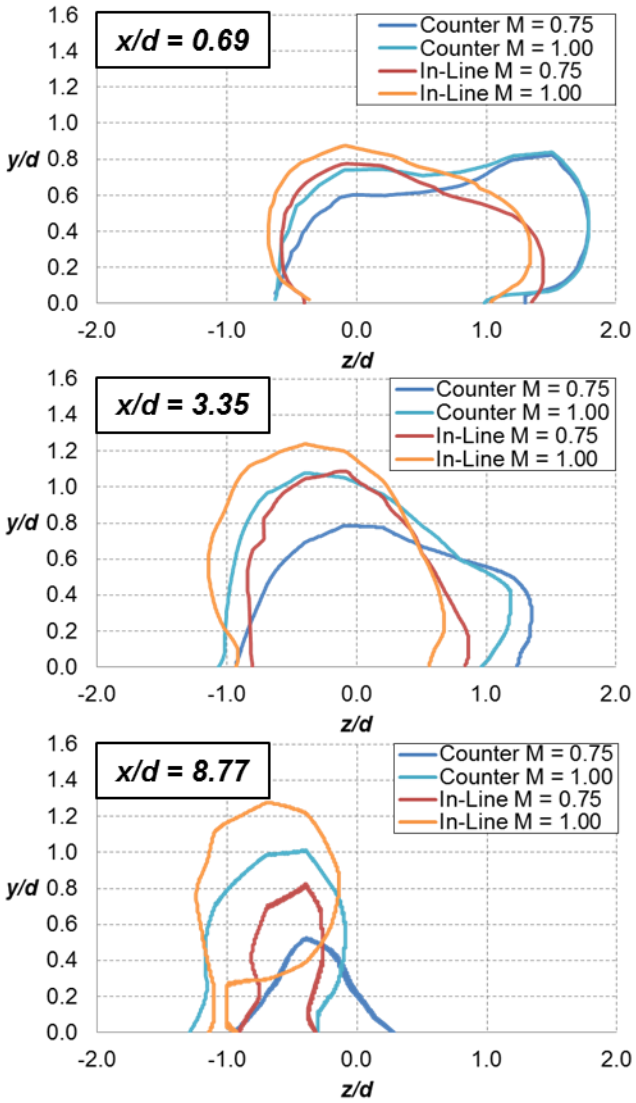

Figure 14: Contour lines for θ = 0.25 for all conditions

Table 1: Laterally averaged η for all conditions and stream-wise locations tested in this study [18]

	x/d =	0.7	3.4	8.8
M		Laterally averaged η		
0.75	Counter	0.12	0.15	0.13
0.75	In-line	0.10	0.13	0.11
1.00	Counter	0.08	0.15	0.13
1.00	In-line	0.05	0.10	0.09

In the measured laterally averaged adiabatic effectiveness results presented in Table 1, there was a drop-off in effectiveness for the in-line case between M = 0.75 and 1.00, while there was a minimal change in effectiveness for the counter flow case between these two blowing ratios. A reduction in adiabatic effectiveness with increasing blowing ratio typically indicates that the jet is separating from the wall due to the increased momentum of the coolant. This result suggests that the in-line jet is separating more than the counter flow jet. However, Figure 13 shows that, at the jet centerline, the position of the maximum θ peak above the wall is similar for the counter and in-line cross-flow cases for M = 1.0, indicating similar separation for both cases. Examining the contour plots in Figure 12 shows that while the centerline of the jet core of the counter jets lifts off from the wall with increasing blowing ratio, there is little change in the y-location of the center of the downstream bulge. Figure 14 makes this result clearer by plotting the θ = 0.25 contour lines for the different blowing conditions and stream-wise locations with respect to each other. At the upstream location, x/d = 0.69, even though the footprints at the wall were similar for the counter and in-line counter-flow cases, the counter cross-flow cases had distinct bulges on the right side of the coolant jets that did not occur for the in-line cases. Farther downstream at x/d = 3.35, the extent of the right side bulge for the counter cross-flow case has decreased, but the bulge has moved closer to the wall resulting in a wider adiabatic effectiveness footprint for the counter flow case. At the far downstream location, x/d = 8.77, the right side bulge has disappeared, but the counter cross-flow case maintains a wider adiabatic effectiveness footprint. The cores of the counter cross-flow coolant jets also appear closer to the wall, suggesting less separation for the counter cross-flow cases. These results suggests that the downstream jet bulge and its associated vortex structure help keep the jet attached to the wall for the counter flow case, while the in-line jet is more susceptible to separation with increasing blowing ratio.

CONCLUSIONS

Thermal field measurements were made for round compound angle holes fed by a cross-flow in order to examine the effects of the direction of internal cross-flow on the effectiveness of the coolant jets. Blowing ratios causing peak adiabatic effectiveness (M = 0.75 and 1.00) were studied at a density ratio of DR = 1.5. Previous measurements of adiabatic effectiveness showed that internal cross-flow counter to the direction of coolant injection caused higher peak adiabatic effectiveness levels than cross-flow in-line with the direction of coolant injection. This study is the first in the open literature to perform thermal field measurements to provide insight into this effect.

It was shown that the improvement in adiabatic effectiveness for counter cross-flow over in-line cross-flow was caused by the formation of a bulge that formed on the downstream side of the compound angle coolant jet when fed by counter cross-flow. This flow structure did not form for in-line cross-flow. The downstream bulge was shown to have properties favorable to film cooling in that it tended to attach to the wall as it moved downstream and was resistant to separation from the wall with increased blowing relative to the in-line jets and the primary core of the counter jet.

The root cause of the favorable behavior of the counter cross-flow jet was most likely the increased separation region that developed at the entrance of the film cooling hole due to the sharp turning angle required for the coolant to enter the hole. The larger separation region likely led to increased turbulence and a skewed velocity profile at the exit of the hole that contributed to the development of vortices that encouraged the favorable behavior of this jet. Highly resolved velocity field measurements are still needed in the near hole region to provide a more complete understanding of the behavior of these coolant jets.

ACKNOWLEDGMENTS

The authors are grateful for the continued financial and technical support from GE Aviation and GE Global Research.

REFERENCES

[1] Bunker, R. S., 2005, “A Review of Shaped Hole Turbine Film-Cooling Technology,” *J. Heat Transfer*, Vol. 127, pp. 441-453.

[2] Schmidt, D., Sen, B., and Bogard, D., 1996, “Film Cooling with Compound Angle Holes: Adiabatic Effectiveness,” *J. Turbomach.*, Vol. 118, pp. 807–813.

[3] Goldstein, R.J. and Jin, P., 2001, “Film Cooling Downstream of a Row of Discrete Holes With Compound Angle,” *J. Turbomach.*, Vol. 123, pp. 222–230.

[4] Ligrani, P. M., Wigle, J. M., and Jackson, S. W., 1994, “Film-Cooling from Holes with Compound Angle Orientations: Part 2 – Results Downstream of a Single Row of Holes with 6d Spanwise Spacing,” ASME *Journal of Heat Transfer,* Vol. 116, pp 353-362.

[5] Jung, I.S. and Lee, J.S., 2000, “Effects of Orientation Angles on Film Cooling Over a Flat Plate: Boundary Layer Temperature Distributions and Adiabatic Film Cooling Effectiveness,” *J. Turbomach.*, Vol. 122, pp. 153-160.

[6] Andreopoulos, J., Rodi, W., 1984, "Experimental Investigation of Jets in a Crossflow." *J. Fluid Mech., Vol.* 138, pp. 93-127.

[7] Pietrzyk, J. R., Bogard, D. G., Crawford, M. E., 1989, "Hydrodynamic Measurements of Jets in Crossflow for Gas Turbine Film Cooling Applications." *J. Turbomach.*, Vol. 111, pp. 139-145.

[8] Leylek, J. H., Zerkle, R. D., 1994, "Discrete-Jet Film Cooling: A Comparison of Computuational Results With Experiments." *J. Turbomach.*, Vol. 116, pp. 358-368.

[9] Walters, D. K., Leylek, J. H., 2000, "A Detailed Analysis of Film-Cooling Physics: Part I - Streamwise Injection With Cylindrical Holes." *J. Turbomach*., Vol. 122, pp. 102-112.

[10] McGovern, K. T., Leylek, J. H., 2000, "A Detailed Analysis of Film Cooling Physics: Part II - Compound-Angle Injection With Cylindrical Holes." *J. Turbomach*., Vol. 122, pp. 113-120.

[11] Thole, K. A., Gritsch, M., Schulz, A., and Wittig, S., 1997, "Effect of a Crossflow at the Entrance to a Film-Cooling Hole," *Journal of Fluids Engineering*, Vol. 119, pp. 533-540.

[12] Gritsch, M., Schulz, A., Wittig, S., 1998, "Adiabatic Wall Effectiveness Measurements of Film-Cooling Holes With Expanded Exits." *J. Turbomach.*, Vol. 120, pp. 549-556.

[13] Gritsch, M., Schulz, A., and Wittig, S., 2003, "Effect of Internal Coolant Crossflow on the Effectiveness of Shaped Film-Cooling Holes," *J. Turbomach.*, Vol. 125, pp. 547-554.

[14] Saumweber, C., and Schulz, A., 2008, "Comparison of the Cooling Performance of Cylindrical and Fan-Shaped Cooling Holes with Special Emphasis on the Effect of Internal Coolant Cross-Flow," ASME paper GT2008-51036, Berlin, Germany.

[15] Dees, J. E., Bogard, D. G., Ledezma, G. A., and Laskowski, G. M., 2011, "Overall and Adiabatic Effectiveness on a Scaled Up, Simulated Gas Turbine Vane: Part I – Experimental Measurements," ASME paper GT2011-46612, Vancouver, Canada.

[16] Dees, J. E., Bogard, D. G., Ledezma, G. A., and Laskowski, G. M., 2011, "The Effects of Conjugate Heat Transfer on the Thermal Field Above a Film Cooled Wall," ASME paper GT2011-46617, Vancouver, Canada.

[17] Peng, W., Jiang, P. X., 2012 "Experimental and Numerical Study of Film Cooling with Internal Coolant Cross-Flow Effects." *Experimental Heat Transfer*, Vol. 25, pp. 282-300.

[18] McClintic, J. W., Klavetter, S. R., Winka, J. R., Anderson, J. B., Bogard, D. G., Dees, J. E., Laskowski, G. M., and Briggs, R., 2015, "The Effect of Internal Cross-Flow on the Adiabatic Effectiveness of Compound Angle Film-Cooling Holes," *J. Turbomach.*, Vol. 137, 071006.

[19] Klavetter, S. R., "Internal Crossflow Effects on Turbine Airfoil Cooling Adiabatic Effectiveness with Compound Angle Round Holes," Master's Thesis, The University of Texas at Austin, 2014.

[20] Stewart, W. R. and Bogard, D. G., 2014, "Experimental Thermal Field Measurements of Film Cooling Above the Suction Side of a Turbine Vane," ASME paper GT2014-25975, Düsseldorf, Germany.

[21] Cutbirth, J. M. and Bogard, D. G., 2002, "Evaluation of Pressure Side Film Cooling with Flow and Thermal Field Measurements – Part II: Turbulence Effects," *J. Turbomach.*, Vol. 124, pp. 678-685.

[22] Moffat, R. J., 1985, "Using Uncertainty Analysis in the Planning of an Experiment," *J. Fluids Eng.*, Vol. 107, pp. 173-178.